VI International Conference on Computational Methods in Marine Engineering
MARINE 2015
F. Salvatore, R. Broglia and R. Muscari (Eds)

# Numerical Study on Active and Passive Trailing Edge Morphing Applied to a Multi-MW Wind Turbine Section

**A. CORSINI*†, A. CASTORRINI*, M. BOEZI*, F.RISPOLI***

*Sapienza University of Rome, Dept. of Mechanical and Aerospace Engineering,
Via Eudossiana 18, 00184 Roma, Italy.
Tel: +39 0644585231

† SED Soluzioni Energia e Diagnostica Srl,
Via Asi Consortile 7, 03013 Ferentino, Italy

**Key words:** Wind turbine, morphing, airfoil, fluid-structure interaction

**Abstract.** A progressive increasing in turbine dimension has characterized the technological development in offshore wind energy utilization. This aspect reflects on the growing in blade length and weight. For very large turbines, the standard control systems may not be optimal to give the best performance and the best vibratory load damping, keeping the condition of maximum energy production. For this reason, some new solutions have been proposed in research. One of these is the possibility of morphs the blade surface in an active way (increasing the performance in low wind region) or passive (load reduction) way.

In this work, we present a numerical study on the active and passive trailing edge morphing, applied to large wind turbines. In particular, the study focuses on the aerodynamic response of a midspan blade section, in terms of fluid structure interaction (FSI) and driven surface deformation.

We test the active system in a simple start-up procedure and the passive system in a power production with turbulent wind conditions, that is, two situations in which we expect these systems could improve the performance.

All the computations are carried out with a FSI code, which couples a 2D-CFD solver, a moving mesh solver (both implemented in OpenFOAM library) and a FEM solver.
We evaluate all the boundary conditions to apply in the section problem by simulating the 5MW NREL wind turbine with the NREL CAE-tools developed for wind turbine simulation.

## 1 INTRODUCTION

During the last twenty years, the development process on wind turbines have led to an increment in size of the rotor. As an effect of this, the maximum operating turbine sizes reaches 5-6 MW in nominal power, with blade length of 60 or more meters. These particular dimensions are designed specially for offshore applications, because of the transportation problem associated to large structures.

Considering this rotating system, phenomena directly involved with the life cycle and performance evolution are not simple to be predicted and the current experience does not allow to know in advance how these structures behave over long periods. Indeed, several factors influence the velocity in a certain point of the rotor vain:

- Atmospheric boundary layer;

- Small turbulent scale fluctuation;
- Wind gusts;
- Interaction between fluid and rotor blade.

The aerodynamic state resulting from these phenomena is unsteady, and it presents a variable inflow velocity, which involves a variation of the angle of attack at the section level, connected to a variation of the aerodynamic load. This fluctuation implies the occurrence of fatigue load in the rotor vain, but also inside the structural components of the wind turbine, as the transmission system. This aspect is relevant also in terms of expected rotor performance; in fact, the aerodynamic surface is usually designed with BEM methods, which take into account mainly the steady behavior of the airfoils.

A possible solution that can be useful for damping these oscillations and better managing the flow variability is to use a variable geometry in the blade, based on the concept of smart blade (see for example [1]).

In the present work, authors present a numerical study on the active and passive trailing edge morphing. In particular, the study focuses on the aerodynamic response of a midspan blade section, in terms of FSI and driven surface deformation.

In this context, numerical simulations can be an important tool for studying all these aspects, starting from the design phase. Thus, a correct modeling of the phenomena associated to this problem is crucial.

In order to contextualize the 2D problem, authors used as flow condition the local aerodynamic quantities recorded for the same section, using the NREL wind turbine simulator FAST, applied to simulate the 5MW NREL wind turbine. The two systems have two different operating logic, thus they require to be evaluated in two different conditions. We simulate the passive system in a turbulent wind, while the active system follows a simple start-up procedure.

The passive system was modelled and solved through a FSI iterative algorithm, which strongly combines the solution of fluid phase, solid phase and mesh motion. The turbulence simulator TurbSim was used to obtain the wind input for FAST in order to obtain the local aerodynamic quantities corresponding to an IEC Normal Turbulence Model.

The active morphing was simulated using the same model described above, imposing a time-varying deformation of the trailing edge surface.

The Fluid Structure Interaction (FSI) analysis could be a useful instrument in terms of:

- Quantification of the structural response to given flow condition.
- Classification of the mechanism underlying the coupling between fluid and structure.
- Characterization of the fatigue in the structure.
- Design properties to minimize the self-induced vibrations.

This is the reason why many authors developed different strategies for FSI resolution problem. Generally, there are two ways in the state of the art to approach the problem. The first uses a fully coupled (monolithic) scheme. In this way, it is possible to solve complex analyzes based on nonlinear equations. The adjective "monolithic" is used to identify a global process of discretization related to fluid and structural domain. In [2], [3], [4], it is possible to find application of this approach developed by Hubner (2004), Walhorn (2005) and Tezduyar (2006).

Another point of view that characterizes the FSI resolution process requires the application of a partitioned scheme. In this way, authors are able to use a specific solver for each region of the domain. The interaction between fluid and solid region is managed by the boundary conditions of the specific solver. The partitioned approach is based on the possibility to apply a specific solver that represents the state-of-art for each physic domain. Following this logic it is possible to develop an efficient global algorithm, with different grid resolution in the coupling interface between the two domains. Nevertheless, this aspect has to be considered in a particular way, especially during the information transfer process, in the interface zone between different solvers. The idea behind this study is to solve consecutively in each time interval the different physical domains. Authors in [6], [7] and [8] summarize some "partitioned" approaches.

Establishing a comparison between these two schemes is not a simple task, however, in [9] Degroote (2008) analyzes the behavior of this resolution methods using the same process of discretization. The main result of this analysis is related to the lower computational load required by "partitioned" approach then the "monolithic" one. This difference is considerable if we considerate that the accuracy of the result obtained by these methods is comparable.

We apply a "partitioned implicit" FSI approach, because the monolithic approach is highly recommended for FSI problems where the stiffness of the structure is very low and the densities between fluid and solid phase are comparable. Indeed, in wind turbine application the physical difference between solid and fluid phase is sufficient to guarantee that a staggered algorithm is an efficient choice.

The fluid solver solves the Unsteady Reynolds Averaged Navier-Stokes equations of an incompressible flow, with a k-ε turbulence model. The Arbitrary Lagrangian-Eulerian formulation was used to take into account the mesh deformation and velocity. A frame of linear elastic beams modelled the structure, while the mesh motion was carried out by the solution of the Laplace equation. Furthermore, the Aitkien relaxation method is used to improve the stability.

The numerical simulations were performed using an in-house coupling solver, which combine the open-source library OpenFOAM (PISO algorithm and moving mesh) and an in-house FEM code for the dynamic solution of the frame structures.

## 2 METHODOLOGY

The method proposed in the present study consists of a systematic approach, which we can synthesize in the following points.

- The unsteady flow around the airfoil is solved with a CFD computation;

$$F\left(\mathbf{d}^{n+1}, t^{n+1}, \mathbf{v}^{n+1}\right) = \mathbf{f}^{F} \tag{1}$$

The flow solution is used to obtain the fluid's traction vector on the coupled boundary δT applied as boundary condition on force load $\mathbf{f}^{S}\left(t^{n+1}\right)$

- From the boundary condition $\mathbf{f}^S\left(t^{n+1}\right)$ it is possible to solve the solid domain;

$$S\left(\mathbf{d}^{n+1}\right) = \mathbf{f}^S\left(t^{n+1}\right) \tag{1}$$

- the displacement vector d, from solid grid, is used to translate the boundary of the fluid. This step is also known as *Dirichlet transfer step*. The fluid mesh has to be moved accordingly to $\Delta d = 0$. This is the hypothesis of pseudo-solid approximation applied to the fluid mesh.

- This cycle should be repeated until convergence achieved, where the predicted displacement field is consistent with given pressure difference;

$$\tilde{d} = S^{-1}\left(F\left(d^{n+1}\right)\right) = d^{n+1} \tag{3}$$

The Aitken relaxation method (see [5]) was introduced in order to accelerate the convergence in the sub-cycle.

## 3 NUMERICAL SCHEMES

### 3.1 Fluid phase solver

The solution of the unsteady flow field around the airfoil is a necessary starting point for the FSI simulation. We obtain the flow field solution by performing a CFD unsteady simulation of the single airfoil in a two-dimensional domain. The computational domain is an O-type grid, subdivided in two main areas. The points of the mesh zone associated to the trailing edge are able to move.

We use OpenFOAM 2.1 [10], an open source finite volume computational fluid dynamic code, for all the fluid phase computations.

The CFD solver applied for the purpose of this work is based on a differential approach for the resolution of the turbulent flow; Pressure Implicit with Splitting of Operators (PISO) implemented in OpenFOAM, which is applied to solve the unsteady RANS equations for an incompressible fluid.

The turbulence model used in this work is the high-Reynolds number k-ε, with wall functions modelled at the wall boundary.

PISO algorithm consists in a single implicit momentum equation predictor followed by several step of pressure evaluations and explicit velocity corrections.

### 3.2 Structure solver

We approximate the solid domain with a frame structure, composed of one-dimensional beam elements. The final system of equations is obtained by the application of the *direct stiffness method*. As reported in literature [11], the correct application of this method is based on the evaluation of the mechanical properties of the elements that compose the structure. These parameters are required to identify the *element stiffness and mass matrices* ($[K]^e$, $[M]^e$), which are based on the shape function of the Euler-Bernoulli beam. The FEM code is able to considerate elements configurations, in terms of orientation and connections in the global

reference. The application of a coupling matrix is used to assign the prescribed boundary conditions to the system equations.

The model performs dynamic analysis, following the Newmark's approach. This method is based on a time discretization with constant interval $\Delta t$. Starting from the initial configuration of the system, for each time step the following equilibrium equation is solved:

$$\mathbf{Ma}(t)+\mathbf{Ku}(t)=\mathbf{f}(t) \tag{4}$$

When the **M** term is used to identify the *global mass matrix*, which is assembled using the *direct method* [11]. In Newmark's scheme, the following time linear form expresses the acceleration term on nodes:

$$\ddot{\mathbf{u}}(t)=\mathbf{a}(t)=\mathbf{a}_{\mathbf{j}}+\frac{t-t_j}{\Delta t}\left(\mathbf{a}_{\mathbf{j+1}}-\mathbf{a}_{\mathbf{j}}\right) \tag{5}$$

The integration of the relation above is useful to predict the velocity and displacement trend of the system.

$$\dot{\mathbf{u}}(t)=\mathbf{v}(t)=\mathbf{v}_{\mathbf{j}}+\left(t-t_j\right)\mathbf{a}_{\mathbf{j}}+\frac{\left(t-t_j\right)^2}{2\Delta t}\left(\mathbf{a}_{\mathbf{j+1}}-\mathbf{a}_{\mathbf{j}}\right) \tag{6}$$

$$\mathbf{u}(t)=\mathbf{u}_{\mathbf{j}}+\left(t-t_j\right)\mathbf{v}_{\mathbf{j}}+\frac{\left(t-t_j\right)^2}{2}\mathbf{a}_{\mathbf{j}}+\frac{\left(t-t_j\right)^3}{6\Delta t}\left(\mathbf{a}_{\mathbf{j+1}}-\mathbf{a}_{\mathbf{j}}\right) \tag{7}$$

### 3.3 FSI convergence

In order to stabilize the convergence process in the FSI algorithm, we introduced Aitkens relaxation procedure on the Dirichlet transfer step (an example of use is in [5]). This method can be considered as a generalization of the secant method.

In the Aitken model the variation term is described by the following equation,

$$\Delta \mathrm{x}=\omega_{\mathrm{n+1}}\left(\mathrm{x}^{*}_{\mathrm{n+1}}-\mathrm{x}_{\mathrm{n}}\right)+\left(1-\omega_{\mathrm{n+1}}\right)\left(\mathrm{x}_{\mathrm{n}}-\mathrm{x}_{\mathrm{n-1}}\right). \tag{8}$$

The underrelaxation factor ( $\omega_{\mathrm{n}}$ ) is then modified for the next step as $\omega_{\mathrm{n+1}}=\gamma_{\mathrm{n}}\omega_{\mathrm{n}}$, when the $\gamma_{\mathrm{n}}$ term is obtained by the application of the secant method.

$$\gamma_{\mathrm{n}}=-\frac{\left(\mathrm{x}_{\mathrm{n}}-\mathrm{x}_{\mathrm{n-1}}\right)}{\left\|\left(\mathrm{x}^{*}_{\mathrm{n+1}}-\mathrm{x}_{\mathrm{n}}\right)-\left(\mathrm{x}_{\mathrm{n}}-\mathrm{x}_{\mathrm{n-1}}\right)\right\|^2}\cdot\left(\mathrm{x}^{*}_{\mathrm{n+1}}-\mathrm{x}_{\mathrm{n}}\right) \tag{9}$$

## 4 PROBLEM SET-UP

The cases in study correspond to the analysis of two typical way of application of the morphing trailing edge control.

- In active case, analysis of the behavior of an active morphing system, testing it in a symbolic start-up maneuver.
- In passive case, analysis of the behavior of a passive morphing system, in its

application to a generic power production state with a turbulent wind.

We want to verify that the analyzed system and the applications procedures lead to a final solution that effectively produces, in these particular conditions, an increasing of the global performance.

### 4.1 Turbine description

The definition of the baseline wind turbine used as base in this work is reported in [12]. L'origine riferimento non è stata trovata., and corresponds to the 5 MW HAWT designed by the National Renewable Energy Laboratory. Table 1 summarizes the main characteristics of the wind turbine, while Table 2 reports the baseline blade properties.

Table 3 illustrates the aerodynamic design of the blade using the AeroDyn [13] nomenclature. The blade node locations, labeled as “RNodes”, are directed along the blade-pitch axis from the rotor center (apex) to the blade cross sections. The element lengths, “DRNodes,” sum to the total blade length of 61.5 m, divides the wind turbine in 17 section.

"DU" class refers to Delft University and "NACA" refers to National Advisory Committee for Aeronautics.

### 4.2 Reference airfoil

The choice of the reference airfoil come from two main reasons, one is of a physical nature, the other one is related to the modeling adopted. In a wind turbine blade, the midspan sections are critical because they contribute (as the tip region) to the performance, but they also experience an oscillation of the relative wind due to the turbulence. This effect is greater than the effect that the wind turbulence has on the tip region, making the mid region more subjected to aerodynamic load vibrations. Furthermore, the numerical model presented is structured for two-dimensional fluid dynamics and structural domain analysis. This is the reason why it is not possible to gain accurate results, when this solver is applied on the innermost and outermost regions, which are characterized by the presence of secondary flows. These motivations led the authors towards a reference airfoil located in the mid-tip span region, and in particular, located on the 12th nodal position of Table 3. At this position, we can find a classical NACA 64517 airfoil.

**Table 1.** Turbine data

| | |
|---|---|
| RATING | 5 MW |
| ROTOR ORIENTATION, CONFIGURATION | Upwind, 3 Blades |
| CONTROL | Variable Speed, Collective Pitch |
| ROTOR, HUB DIAMETER | 126 m, 3m |
| HUB HEIGHT | 90 m |
| CUT – IN, RATED, CUT – OUT WIND SPEED | 3 m/s, 11.4 m/s, 25 m/s |
| CUT – IN, RATED ROTOR SPEED | 6.9 rpm, 12.1 rpm |

**Table 2.** Blade data

| | |
|---|---|
| LENGHT | 61.5 m |
| OVERALL MASS | 17’740 kg |

**Table 3.** Blade sections data

| Node (-) | RNodes (m) | DRNodes (m) | Chord (m) | Airfoil Profile (m) |
|---|---|---|---|---|
| 1 | 2.8667 | 2.7333 | 3.542 | Cylinder_1 |
| 2 | 5.6000 | 2.7333 | 3.854 | Cylinder_1 |
| 3 | 8.3333 | 2.7333 | 4.167 | Cylinder_2 |
| 4 | 11.7500 | 4.1000 | 4.557 | DU40_A17 |
| 5 | 15.8500 | 4.1000 | 4.652 | DU35_A17 |
| 6 | 19.9500 | 4.1000 | 4.458 | DU35_A17 |
| 7 | 24.0500 | 4.1000 | 4.249 | DU30_A17 |
| 8 | 28.1500 | 4.1000 | 4.007 | DU25_A17 |
| 9 | 32.2500 | 4.1000 | 3.748 | DU25_A17 |
| 10 | 36.3500 | 4.1000 | 3.502 | DU21_A17 |
| 11 | 40.4500 | 4.1000 | 3.256 | DU21_A17 |
| 12 | 44.5500 | 4.1000 | 3.010 | NACA64_A17 |
| 13 | 48.6500 | 4.1000 | 2.764 | NACA64_A17 |
| 14 | 52.7500 | 4.1000 | 2.518 | NACA64_A17 |
| 15 | 56.1667 | 2.7333 | 2.313 | NACA64_A17 |
| 16 | 58.9000 | 2.7333 | 2.086 | NACA64_A17 |
| 17 | 61.6333 | 2.7333 | 1.419 | NACA64_A17 |

### 4.3 Active case analysis description

We are interested in the performance estimation of the starting maneuver of the wind turbine, related to an application of an active morphing concept, applied on the trailing edge of the airfoil.

We superimpose the trailing edge deformation as a function of the expected relative wind velocity. The deformation was achieved through a simple parabolic shape function applied to the trailing edge coordinates.

The active morphing process starts from the full-deformed configuration, corresponding to the cut-in relative wind speed, and finishes in the undeformed configuration at the nominal relative wind speed.

The section is subjected to the velocity path reported in Figure 3, characterized by a relative wind starting velocity from 5 m/s (rotor stopped and cut-in wind velocity), to reach the nominal operating point condition linearly.

During the evolution process, the angle of attack is kept constant, exploiting the variable speed control system, reported in Table 1. In this way, it is possible to preserve similar triangle input speed of the wind turbine. Figure 2 shows the morphing process evolution. The airfoil trailing edge area was rotated by 3 degrees upwards. In this case, the trailing edge deflection rate is considered constant.

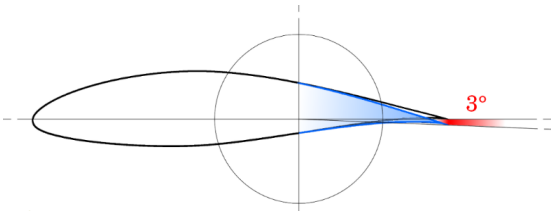


**Figure 1.** Active morphing, configuration at t = 0 s

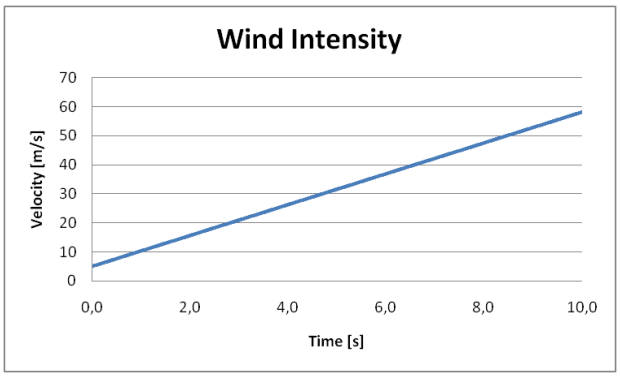


**Figure 2.** Relative wind velocity considered in the start-up case

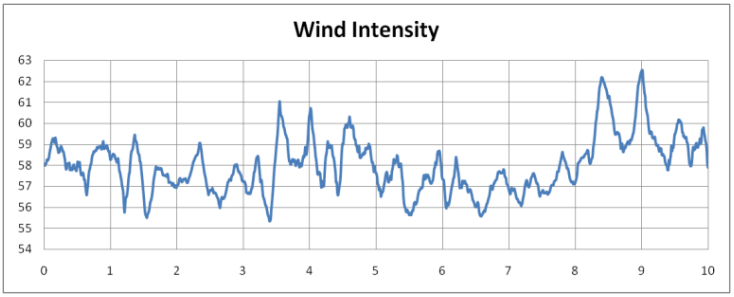


**Figure 3.** Section relative wind velocity, computed for the passive morphing case

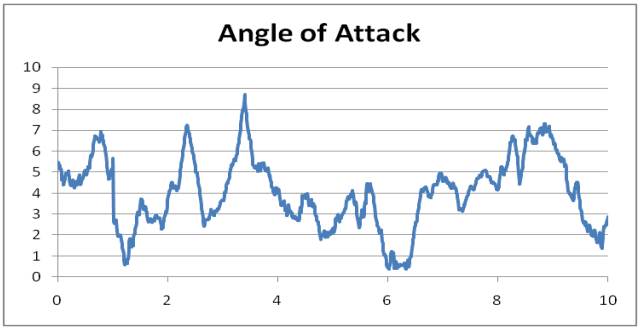


**Figure 4**. Section angle of attack, computed for the passive morphing case

### 5.2 Passive case analysis description

Here we want to estimate the response due to the passive trailing edge morphing system, when the airfoil is subjected to a variable input velocity, which simulates the typical turbulence scenario in the nominal operating point of the wind turbine.
The turbulence simulator TurbSim [14] was used to obtain the wind input for FAST [15] in order to obtain the local aerodynamic quantities corresponding to an IEC-NTM (Normal Turbulence Model) [16]. After that, we take the relative wind velocity magnitude (Figure 4) and local angle of attack (Figure 5) at the corresponding section. Finally, we applied this velocity profile using a tabular velocity input at the inlet boundary of the CFD domain.

### 5.2 Fluid mesh and boundary conditions

The topologic grid type adapted is a special "O-type" construction with an average radius of about 80 chords. In this way, it is possible to identify two different areas, with different boundary conditions. In the specific, authors decided to apply a *fixed-wall* and a *moving-wall* region, the last one starts from the 60 % of the chord length until the trailing edge. The mesh domain counts 1.4E+04 hexahedral cells assembled in a structured way. The coupled interface is characterized by a $y^+$ dimension of 60, related to a $\Delta\mathbf{s}$ of 1.5E-04 m.

Standard boundary conditions were applied to the RANS computations of incompressible flow (Table 4).

| | |
|---|---|
| *Inflow* | $V_0$ = 12 m/s; TI = 5%; Time varying velocity; |
| *Outflow* | Zero gradient |
| *Fixed wall* | No-slip condition |
| *Moving wall* | No-slip condition |
| *Radial far field* | Zero gradient |

**Table 4. Fluid phase boundary conditions.**

All computations utilize a second order linear upwind divergence scheme, with a convergence tolerance of $10^{-7}$ for all computed quantities.
For the stability of the computation process, authors used specifics relaxation factors for the main computational variables as showed in Table 5.

| | |
|---|---|
| *k, epsilon* | 0.5 |
| *p* | 0.3 |
| *u* | 0.7 |

**Table 5. Relaxation Factors**

### 5.2 Solid mesh and boundary conditions

To realize the truss used in the trailing edge morphing process, the inside part of the airfoil profile was modeled through the frame structure shown in Figure 6.

We applied different mechanical properties to obtain an automatic response in term of displacement, considering the induced stresses generated on the airfoil by external conditions. In this way, the airfoil is able to adapt the trailing edge configuration in order to minimize the load magnitude in this area.

We choose the mechanical properties of the solid elements such as to avoid flutter instabilities and deformations magnitude out of the linear deformation field:

- Isotropic material
- Young Modulus: 2 GPa
- Material Density: 1500 kg/m3
- Element Section Area: 0.01 – 0.05 m

It is possible to observe that these properties can be easily obtained with a particular polymeric material, which are of common use in wind turbine technology.

The structure is constrained imposing a zero displacement at the two leftmost nodes.

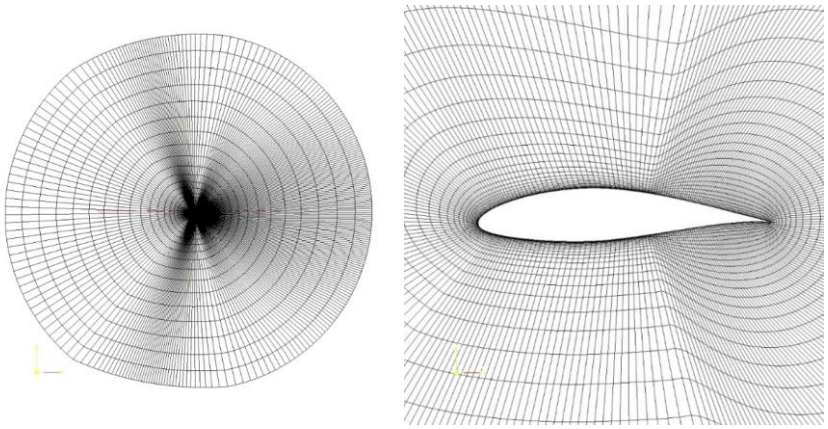

**Figure 5.** Fluid computational domain

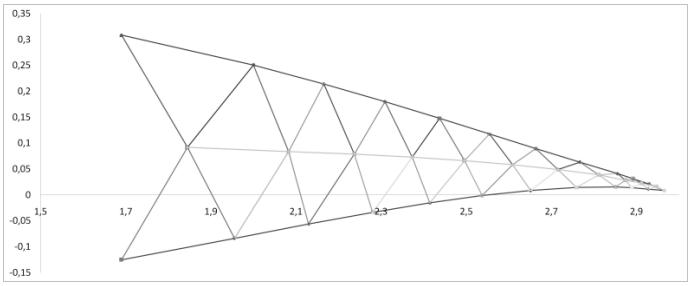


**Figure 6.** Frame structure applied for the trailing edge

## 6 RESULTS

We can observe the results in terms of the main aerodynamic parameters. Figure 7 shows the final comparison in terms of lift coefficient, drag coefficient and their ratio between the standard (rigid) and the morphed configuration of the airfoil in the active case. As expected, the lift coefficient trend for the morphed configuration stands at higher levels than the standard. This difference tends to fade near the nominal operating point, where the airfoil curvature returns toward the original configuration. The drag coefficient trends, in the morphed and standard configuration, are comparable. This is the reason why the aerodynamic efficiency, defined as the ratio CL/CD, assumes a higher value in the morphing configuration.

We must observe before analyze the passive case results that, since the structural model is a linear model, the material and structure choice must be such that the maximum elements deformation is limited to the linear field (little deformations).

Figure 8 shows the result of the lift coefficient for the passive case. As expected, the morphed and the standard configuration show a comparable trend. This is due to the limited area assigned to the morphing process, limited only in trailing edge airfoil region. The main difference in lift production is observable in terms of oscillation amplitude. However, also for this application we can note a decrease in term of drag coefficient, as shown in Figure 8. Figure 8 reports also the aerodynamic efficiency; the morphing configuration in this case can be more efficient than the original airfoil.

We choose to represent a half-second window in this case because of the high frequency associated to the unsteady aerodynamic solution.

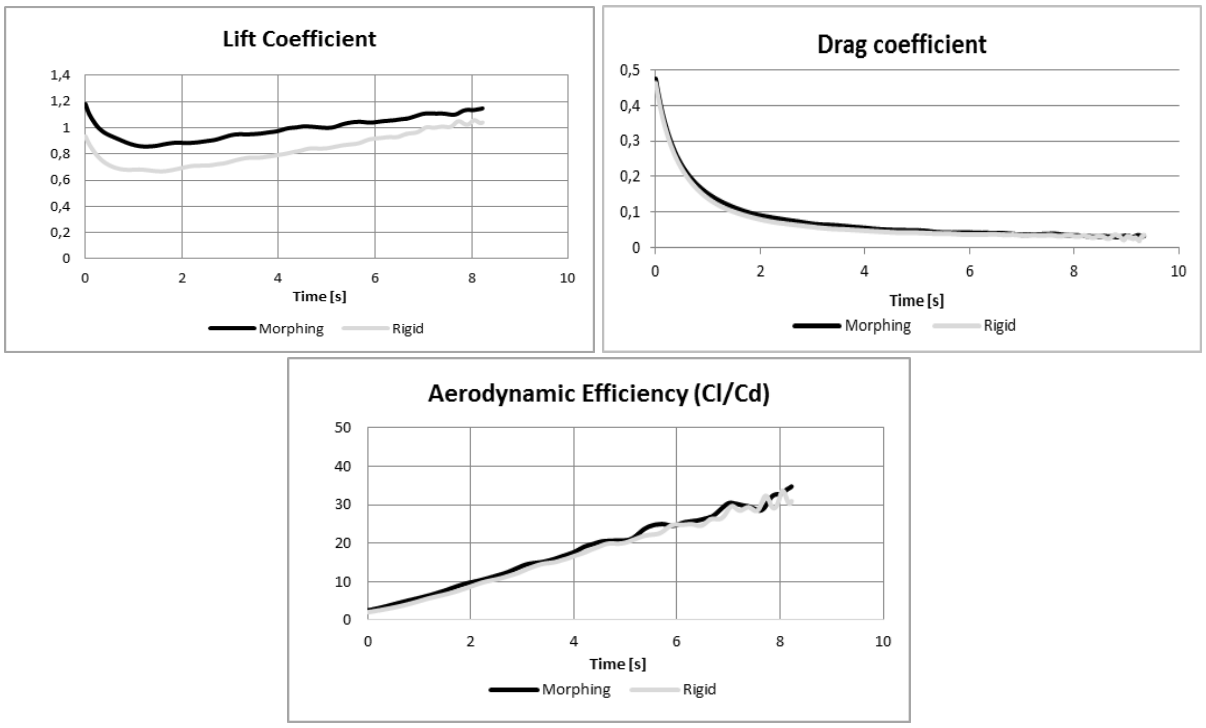


**Figure 7. Active case, aerodynamic coefficients**

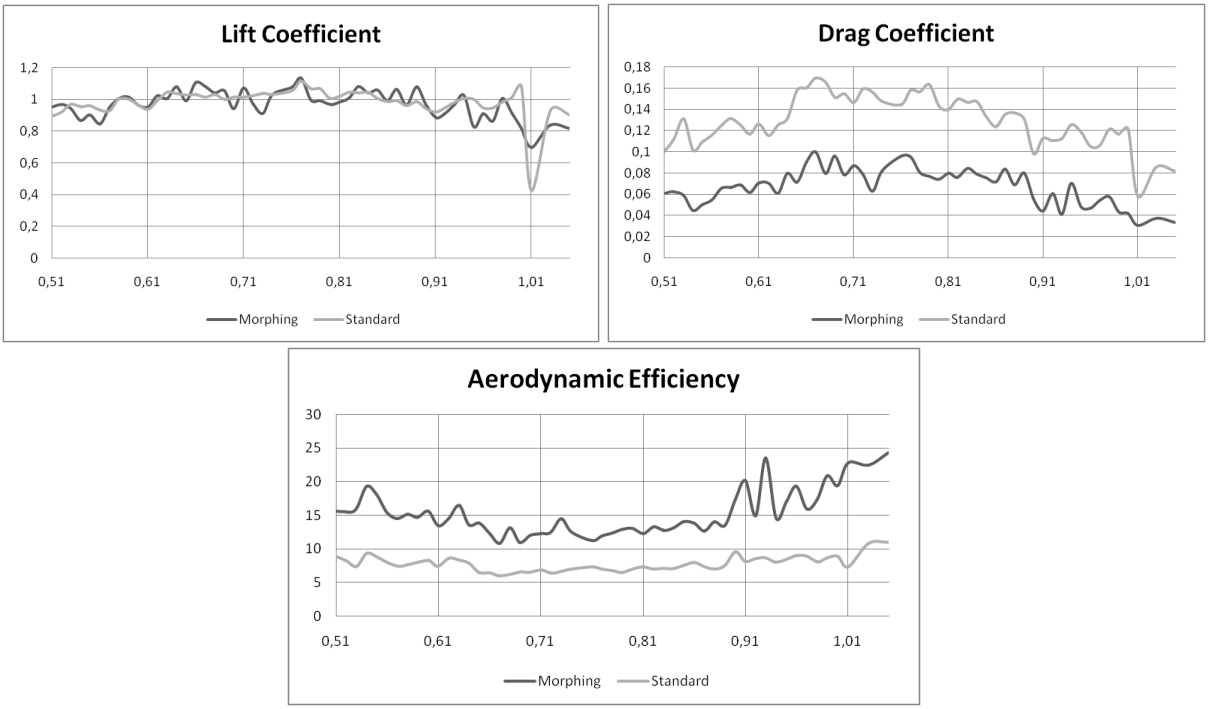


**Figure 8. Passive case, aerodynamic efficiency**

## 7 CONCLUSIONS

We investigate the effect that an active and a passive trailing edge morphing control could have on a section of a large wind turbine.
In order to have an indication of this effect, we choose to simulate the turbine conditions, which we expect are the most significant for the application of these two ways of control. In particular, we simulate a symbolic start-up manoeuver for the active case, and a normal turbulence at the rating wind velocity for the passive case.
The numerical tool used in this analysis is an FSI solver, based on OpenFOAM for moving mesh and fluid dynamics and on a FEM code self-produced. Both the solvers, fluid and structure, were individually validated using state-of-the-art software and experimental results.
The study produces the following results:

- *Active morphing*: in the start-up procedure, the morphed airfoil produces a greater aerodynamic efficiency, as effect of the greater lift coefficient.
- *Passive morphing*: during the power production state, in normal turbulence conditions, the drag of the morphing airfoil is less than the rigid section case. This can be translated in a potential increment in blade torque.

Using a FEM solver based on linear elasticity for the structural displacement, the solution has a limitation on the displacement magnitude. A possible future development can be to study the effect of a big deformation structure, which can be probably useful in terms of vibrational load reduction.

.

## REFERENCES

[1]. Gonzalez L., Rediniotis O., 2005, *"Morphing Wing Using SMA"*, T.I.I.M.S. 3rd Annual Meeting;

[2]. B. Hübner, E. Walhorn and D. Dinkler, Comput. Methods Appl. Mech. Engrg., Vol. 193, pp.2087-2104, 2004.

[3]. T.E. Tezduyar, S. Sathe, R. Keedy, and K. Stein, "Space–time finite element techniques for computation of fluid–structure interactions", Computer Methods in Applied Mechanics and Engineering, 195 (2006) 2002–2027

[4]. Walhorn, Elmar, K¨olke, Andreas, H¨ubner, Bj¨orn, & Dinkler, Dienter. 2005. Fluidstructure coupling within a monolithic model involving free surface flows. Computers and Structures, 83(25-26), 2100–2111.

[5]. M. Barcelos, H. Bavestrello, and K. Maute. A schur-newton-krylov solver for steady-state aeroelastic analysis and design sensitivity analysis. Computer methods in applied mechanics and engineering, 195:2050-2069, 2006.

[6]. Causin, P., J. Gerbeau, and F. Nobile (2005). Added-mass effect in the design of partitioned algorithms for fluid-structure problems. Comput. Methods Appl. Mech. Engrg 194(42-44), 4506–4527.

[7]. C. Farhat and M. Lesoinne, "Two efficient staggered algorithms for the serial and parallel solution of three-dimensional nonlinear transient aeroelastic problems," Computer Methods in Applied Mechanics and Engineering, vol. 182, no. 3-4, pp. 499–515, 2000.

[8]. Fhorster, C., 2007. Robust methods for fluid–structure interaction with stabilised finite elements. Ph.D. thesis, Institut f¨ur Baustatik und Baudynamik, Universit¨at Stuttgart, Germany.

[9]. J. Degroote, K.-J. Bathe, and J. Vierendeels. Performance of a new partitioned procedure versus a monolithic procedure in fluid-structure interaction. Computers & Structures, 87(11– 12):793–801, 2009. DOI: 10.1016/j.compstruc.2008.11.013 SCI-IF: 1.440.

[10]. OpenFoam user guide; URL: http://foam.sourceforge.net/docs/Guides-a4/UserGuide.pdf

[11]. T. J. R. Hughes, E. Cliffs, The finite element method: linear static and dynamic finite element analysis, NJ: Prentice-Hall, (1987), 1985

[12]. J. Jonkman, S. Butterfield, W. Musial, and G. Scott Definition of a 5-MW Reference Wind Turbine for Offshore System Development.

[13]. AeroDyn user manual: *https://nwtc.nrel.gov/AeroDyn*

[14]. TurbSim user manual: *https://nwtc.nrel.gov/TurbSim*

[15]. FAST user manual: *https://nwtc.nrel.gov/FAST8*

[16]. International Standard: IEC61400-1